

Mechanisms of memory storage in a model perirhinal network

Pranit Samarth¹ · John M. Ball¹ · Gunes Unal² · Denis Paré² · Satish S. Nair¹

Received: 2 November 2015 / Accepted: 29 February 2016 / Published online: 12 March 2016
© Springer-Verlag Berlin Heidelberg 2016

Abstract The perirhinal cortex supports recognition and associative memory. Prior unit recording studies revealed that recognition memory involves a reduced responsiveness of perirhinal cells to familiar stimuli whereas associative memory formation is linked to increasing perirhinal responses to paired stimuli. Both effects are thought to depend on perirhinal plasticity but it is unclear how the same network could support these opposite forms of plasticity. However, a recent study showed that when neocortical inputs are repeatedly activated, depression or potentiation could develop, depending on the extent to which the stimulated neocortical activity recruited intrinsic longitudinal connections. We developed a biophysically realistic perirhinal model that reproduced these phenomena and used it to investigate perirhinal mechanisms of associative memory. These analyses revealed that associative plasticity is critically dependent on a specific subset of neurons, termed conjunctive cells (CCs). When the model network was trained with spatially distributed but coincident neocortical inputs, CCs acquired excitatory responses to the paired inputs and conveyed them to distributed

perirhinal sites via longitudinal projections. CC ablation during recall abolished expression of the associative memory. However, CC ablation during training did not prevent memory formation because new CCs emerged, revealing that competitive synaptic interactions governs the formation of CC assemblies.

Keywords Associative memory · Computational model · Synaptic plasticity · Memory retrieval · Perirhinal · Entorhinal

Introduction

The perirhinal cortex occupies a strategic position among temporal lobe structures involved in declarative memory as it relays a large portion of neocortical sensory inputs to the entorhino-hippocampal system and constitutes the main return path for hippocampo-entorhinal efferents to the neocortex (Deacon et al. 1983; Room and Groenewegen 1986; Witter et al. 1986; Insausti et al. 1987; Suzuki and Amaral 1994; Burwell and Amaral 1998a, b). In keeping with this, the perirhinal cortex plays a critical role in high-order perceptual and mnemonic functions. Indeed, perirhinal lesions lead to recognition memory impairments (Gaffan and Murray 1992; Meunier et al. 1993, 1996; Zola-Morgan et al. 1989; Suzuki et al. 1993) that compare to, or are more severe than, those caused by hippocampal and entorhinal lesions (Aggleton et al. 1986; Murray and Mishkin 1986; Meunier et al. 1993; Leonard et al. 1995; Murray et al. 2005). Moreover, perirhinal lesions cause a pronounced associative memory deficit within and across sensory modalities (Murray et al. 1993; Higuchi and Miyashita 1996; Buckley and Gaffan 1998; Parker and Gaffan 1998; Goulet and Murray 2001).

P. Samarth and J. M. Ball both authors contributed equally to this work.

Electronic supplementary material The online version of this article (doi:10.1007/s00429-016-1210-4) contains supplementary material, which is available to authorized users.

✉ Satish S. Nair
nairs@missouri.edu

¹ Division of Biological Sciences and Department of Electrical and Computer Engineering, University of Missouri, Columbia, MO 65211, USA

² Center for Molecular and Behavioral Neuroscience, Rutgers University-Newark, Newark, NJ 07102, USA

What are the perirhinal correlates of memory formation? With respect to recognition memory, perirhinal neurons display reduced responses to visual stimuli that have been presented previously (Brown et al. 1987; Fahy et al. 1993; Li et al. 1993; Miller et al. 1993; Sobotka and Ringo 1993). These response attenuations develop rapidly (within a single training session), last a long time (>1 day), and are far more common among perirhinal than hippocampal neurons (Rolls et al. 1993; Riches et al. 1991; Eichenbaum et al. 1996; Xiang and Brown 1998). In contrast, when monkeys are trained to form associations between two arbitrary visual stimuli, a different behavior emerges. As a result of training, many neurons that were only responsive to one of the stimuli acquire responses to the paired stimulus (Messinger et al. 2001; Naya et al. 2003). Critically, the incidence of such pair coding neurons is much higher in area 36 than in neighboring neocortical regions (Naya et al. 2003).

On the surface, the familiarity-induced response depressions and the emergence of pair coding behavior seem contradictory because both result from repeated presentations of the same stimuli. However, a recent study in the whole brain in vitro (Unal et al. 2012) revealed how synaptic plasticity in the perirhinal network could support these two phenomena, depending on the extent to which the stimulated neocortical activity pattern recruited intrinsic longitudinal perirhinal connections.

Here, we developed a biophysical model of perirhinal area 36 that could reproduce the findings of this in vitro study. We then challenged the model with various spatiotemporally distributed patterns of neocortical inputs to shed light on the mechanisms that support associative memory in the perirhinal network. Our findings suggest that associative memory formation is dependent on the emergence of a specific subset of conjunctive cells that acquire excitatory responses to coincident neocortical inputs and convey their influence to widely distributed perirhinal sites via longitudinal projections.

Methods

Prior computational models of the perirhinal cortex (reviewed in Cowell 2012) have investigated characteristics such as familiarity discrimination (Bogacz and Brown 2003), object recognition (Cowell et al. 2006) and effects of lesions (Cowell et al. 2010). These models used a connectionist formulation with artificial neurons (e.g., Bogacz and Brown 2003), and Kohonen grids (Cowell et al. 2006). In addition, a biologically based neural network model of the inferior temporal cortex was able to reproduce the recency and familiarity effects using calcium-dependent potassium currents and modifiable feedforward synapses,

respectively (Sohal and Hasselmo 2000). Many of these reports emphasized that future studies should aim for biological realism in the design of neuron models. Indeed, there are different approaches to modeling of the nervous system. The approach used here was to develop a model that is as realistic as possible by integrating most of the available experimental information regarding the individual neurons (morphology, passive properties, ionic conductances), their connections, and mechanisms of synaptic plasticity. By definition, because current understanding/knowledge of the perirhinal cortex is incomplete, so will our model. But the objective is to get as close as possible to the real network to study how it implements the function we know it plays. It is possible that simpler networks could reproduce some of these functions. However, the simpler network might achieve the same outcome differently than the real one. Prior to developing the model described below, we explored the ability of simpler models (e.g., firing rate model; Ball et al. 2012) to reproduce perirhinal mechanisms of activity-dependent plasticity. However, we encountered many difficulties (summarized in Section S.8 of the supplementary materials), which led us to the current model.

Overview

Based on experimental data, we created a biophysical model of perirhinal area 36. When lacking relevant data to constrain a particular aspect of the model, we relied on findings obtained in different cortical areas. We first built multi-compartment models of principal and local-circuit neurons based on previously published studies on their electroresponsive properties. Next, principal and local-circuit neurons were distributed in a two-dimensional space that reproduced the structure of perirhinal area 36. Then, we endowed the model with realistic intrinsic and extrinsic connectivity, synaptic conductances and mechanisms of activity-dependent plasticity.

Individual cell models

Principal cell model

In the perirhinal cortex, three main types of principal neurons have been identified: regular spiking (RS), burst firing, and late spiking cells (Beggs and Kairiss 1994; Faulkner and Brown 1999; D'Antuono et al. 2001; Martina et al. 2001b; Moyer et al. 2002). The RS cell type is by far prevalent, except in layer VI where late spiking neurons are more common (Faulkner and Brown 1999; McGann et al. 2001). However, pilot simulations revealed that random synaptic activity in our model network depolarized late-firing cells enough to inactivate the slow A-like current that

underlies the late-firing behavior (Storm 1988), effectively transforming them into RS neurons. Consequently, to accelerate the simulations, we only included principal cells of the RS variety. The RS cell model has five compartments respectively representing the soma (includes axon), basal dendrites, apical trunk, from which emerge two dendritic branches. Their dimensions (Table 1) were selected to preserve biological realism and match passive properties (Table 2; Fig. 1a1; Bush and Sejnowski 1993; Moyer et al. 2002). The ionic currents inserted into each compartment (Table 1, Table S1) were adapted from existing biophysical models of hippocampal and entorhinal neurons (Migliore et al. 1995, 1999; Dickson et al. 2000; Fransen et al. 2002, 2004, 2006; Migliore 2003; Hemond et al. 2008) and tuned to match the electroresponsiveness of principal perirhinal cells, as described in Faulkner and Brown (1999). The inset in Fig. 1a shows how the firing rate of the cells increased with positive current. The principal cells did not generate spike bursts.

Interneuron models

Based on earlier studies in the cerebral cortex (Gupta et al. 2000; Kawaguchi and Kondo 2002; Klausberger and Somogyi 2008), perirhinal area 36 likely contains a wide variety of inhibitory local-circuit cells. However, since

there is limited data about their connectivity and electroresponsive properties (Beggs and Kairiss 1994; Faulkner and Brown 1999; Martina et al. 2001a, b), we only modeled the two types of interneurons that prevail in all cortical regions: parvalbumin-expressing (PV) and somatostatin-expressing (SOM) interneurons, that together account for $\sim 70\%$ of cortical interneurons (Rudy et al. 2011). Other subtypes of local-circuit cells such as those expressing the serotonin ionotropic type 3a receptor (Rudy et al. 2011) had to be left out due to lack of information. For PV and SOM interneurons, we developed three-compartmental models and endowed them with passive properties and voltage-gated-currents (Table 1 and Table S1) so that they could reproduce the electroresponsive properties described in prior experimental studies (Fig. 1a2, a3; Faulkner and Brown 1999; D'Antuono et al. 2001; Martina et al. 2001b; Moyer et al. 2002; Ma et al. 2006).

Connectivity of the model

The perirhinal network model consists of 400 RS, 60 PV and 60 SOM cells distributed in a two-dimensional space with dimensions of 10 and 3 mm for the rostrocaudal and transverse axes, respectively. PV and SOM interneurons were placed at regular intervals along the rostrocaudal axis

Table 1 Model parameters for RS, PV, and SOM cells

Parameter	RS cell		PV cell		SOM cell	
	Soma	Apical trunk/apical/basal dendrites	Soma	Dendrites	Soma	Dendrites
Length (μm)	20	400/300/400	10	150	10	150
Diameter (μm)	10	5/3.5/5	10	5	10	5
E_{leak} (mV)	-78	-78	-82.6	-82.6	-67	-67
E_{Na}	55	55	55	55	55	55
E_{K}	-90	-90	-90	-90	-90	-90
E_{H}	-20	—	—	—	—	—
C_{m} (μF)	0.9	0.9	1.2	1.2	1.6	1.6
g_{leak} (S/cm^2)	$1.585\text{e}-5$	$1.585\text{e}-5$	$5.7\text{e}-5$	$5.7\text{e}-5$	$5\text{e}-5$	$5\text{e}-5$
g_{Kd} (S/cm^2)	0.0001	0.00129/0.00131 (for basal)	0.002	0.002	0.002	0.002
g_{Na} (S/cm^2)	0.8	0.028	0.1	0.05	0.005	0.0042
g_{CaL} (S/cm^2)	0.029	0.0005	—	—	—	—

Additionally, soma had $g_{\text{AHP}} = 0.00028$; $g_{\text{C}} = 0.0108$; $g_{\text{H}} = 1.1\text{e}-5$; and $g_{\text{A}} = 0.0001$

Table 2 Summary of passive electroresponsive properties of RS, PV and SOM cell types

	Biological			Model		
	RS cell	PV cell	SOM ⁺ cell	RS cell	PV cell	SOM cell
Resting membrane potential (mV)	-77.8 ± 0.7	-82.6 ± 1.7	-67.1 ± 2.5	-77.62	-82.6	-67
Input resistance ($\text{M}\Omega$)	300.5 ± 26.3	339.3 ± 47.3	403 ± 39	311.9	351.5	400.4
Membrane time constant (ms)	52.8 ± 2.6	24.3 ± 5.7	33.9 ± 4.1	53.1	21	32

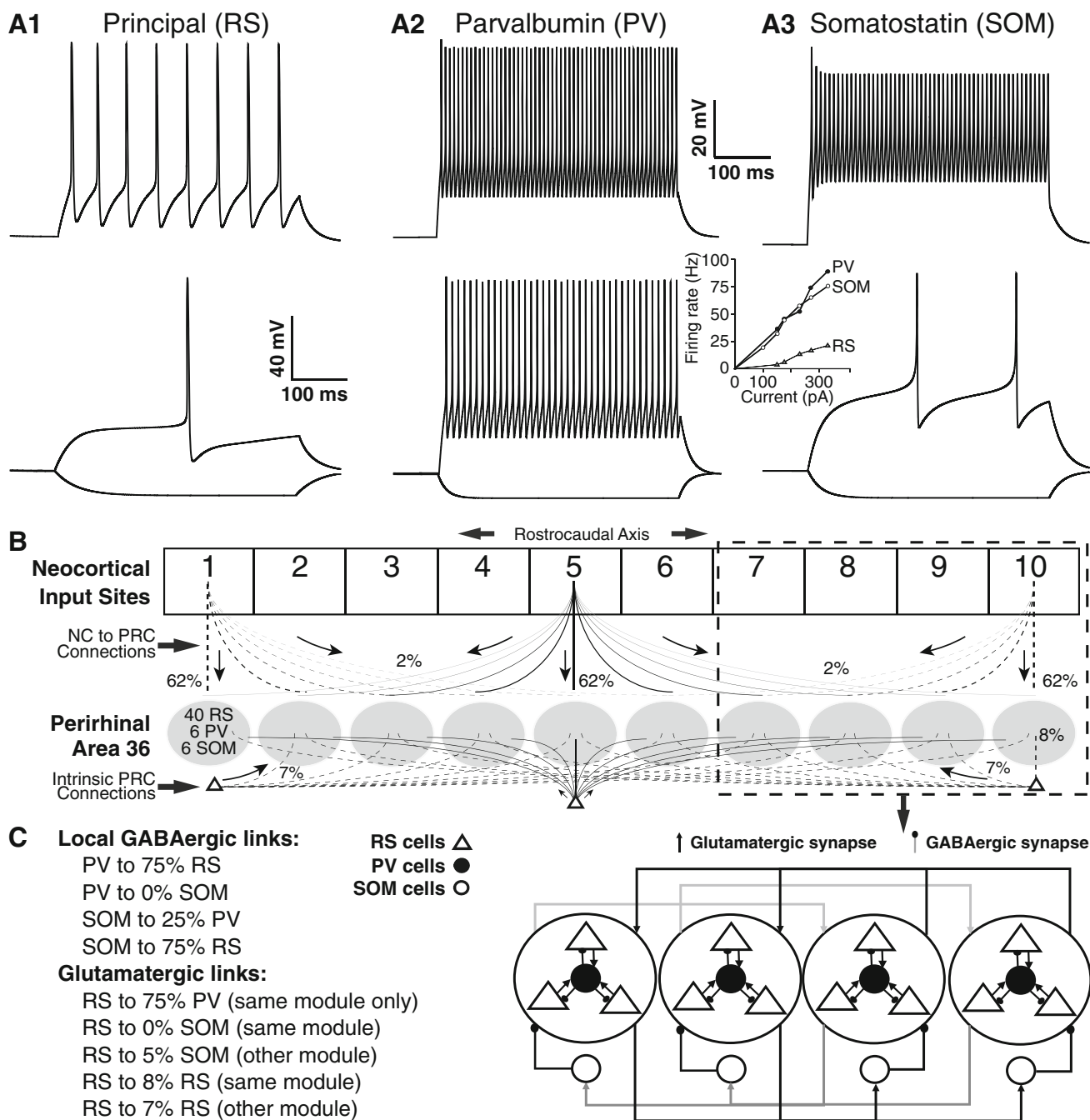


Fig. 1 Physiological properties of model neurons and connectivity of the model. **a** Voltage responses of regular spiking (RS, **a1**), parvalbumin (PV, **a2**), and somatostatin (SOM, **a3**) cells to hyperpolarizing and depolarizing current pulses. All *negative* current pulses have the same amplitude (−100 pA). *Positive* current pulses from *top* to *bottom* are (in pA): RS, 230 and 122; FS, 330, 230; SOM, 400, 67. *Inset* between **a2** and **a3** plots firing rate as a function of injected current in the three cell types. **b** Overall connectivity of perirhinal network model. The model received topographically organized inputs from the neocortex (*top*). Neocortical connections were strongest to

the perirhinal levels in rostrocaudal register (to 62 % of RS cells) and decayed exponentially with distance such that beyond 3 mm, only 2 % of RS cells were contacted by neocortical inputs. In contrast, RS perirhinal neurons contacted a similar proportion of RS cells irrespective of rostrocaudal distance to their targets. Note that there were no spatial discontinuities (*boundaries*) in the perirhinal model. The *gray ellipses* are used for illustration purposes only. **c** Local connectivity of the model. RS cells, *gray triangles*; PV interneurons, *black circles*; SOM interneurons, *white circles*

to ensure uniform inhibition throughout the network. RS cells were also distributed uniformly to make their placement symmetrical with respect to interneurons.

Perirhinal area 36 receives around half of its cortical inputs from a laterally adjacent strip of neocortex termed the “ventral temporal associative neocortex” (Burwell

et al. 1995; Burwell 2000; Furtak et al. 2007). Most of these neocortical inputs end at perirhinal sites rostrocaudally adjacent to their point of origin; only a minority of neocortical axons reach rostrocaudally distant perirhinal sites (Unal et al. 2012). In contrast, the principal perirhinal neurons targeted by neocortical inputs, while also forming local (≤ 1.5 mm; hereafter termed short-range) connections, contribute a prominent system of long-range intrinsic connections that spans the entire rostrocaudal extent of the perirhinal cortex (Witter et al. 1986; Burwell and Amaral 1998a; Biella et al. 2001, 2002; Unal et al. 2012). Long-range neocortical and perirhinal axons only form glutamatergic synapses, prevalently with principal perirhinal neurons (Unal et al. 2013). Also, short vs long-range axons form differential connections with local-circuit cells: the incidence of excitatory synapses onto local-circuit cells is ~ 2 – 3 times lower in long- than short-range connections (Unal et al. 2013). Our perirhinal network model was structured to capture these various properties, as detailed below.

Neocortical inputs

Neocortical afferents were modeled with 201 neocortical input cells distributed along the rostrocaudal extent of the perirhinal network. Each neocortical input formed unique connections with perirhinal neurons and could be activated independently. Note that these “input cells” are in fact just spike trains used for synaptic drive. To constrain the distribution of neocortical inputs to the model, we relied on data from previous physiological studies. In particular, patch recordings of perirhinal cells in horizontal slices kept *in vitro* have revealed that neocortically evoked EPSPs decrease in amplitude as the rostrocaudal distance between the neocortical stimulation site and the recorded cell increases (Martina et al. 2001b). Furthermore, this reduction occurs at different distances from the stimulated neocortical site in RS (3 mm) and PV (1 mm) neurons. Thus, model neocortical connections were structured to reproduce these features (see S.6 in suppl. materials). To ensure uniform neocortical activation of PV interneurons despite the low cell density compared to real cortex, neocortical connections were made to all PV interneurons within 1.0 mm of the neocortical source in the rostrocaudal axis. Neocortical axons did not contact more distant PV cells, in keeping with prior electrophysiological findings (Martina et al. 2001b).

Short- and long-range horizontal connections

A distinguishing property of the perirhinal cortex is the existence of a prominent system of intrinsic longitudinal connections that spans much of its rostrocaudal extent (Witter et al. 1986; Burwell and Amaral 1998a; Biella et al.

2001, 2002). These longitudinal axons arise from and terminate in all layers (Witter et al. 1986; Biella et al. 2001). In the model, long-range connections were made from RS cells to other RS cells located >1.5 mm from the source cell in the rostrocaudal dimension. Long-range connections were not designed to be reciprocal. That is, they were made along the random path of each source cell’s single axon. Each source cell formed 21 such connections along the path of its axon and each target RS cell received ≤ 20 such long-range inputs. This resulted in an RS–RS connection probability of approximately 7 %. Each source cell had only one axon, coursing either rostrally or caudally. For each source cell, the direction of its axon was determined by randomly selecting a first target RS cell. Based on the location of this target cell, either rostral or caudal to the input cell, the path of the axon was chosen, and all other connections were made in that direction. These other connections were determined by randomly selecting 20 additional target cells for a total of 21. A RS cell also made long-range connections to SOM cells with a 5 % connection probability if the latter was connected to an RS cell that received a long-range connection from the same source RS cell. For short-range connections between RS cells, a connection was made with 8 % probability if the rostrocaudal distance between the cells was less than 1 mm. Finally, the model featured realistic conduction delays based on prior experimental observations (Pelletier and Pare 2002; See Suppl. Materials).

Local-circuit inhibitory connections

Lacking perirhinal data to constrain the connections of RS and PV cells, we adjusted these connections to reproduce the dramatic impact of feedforward and feedback inhibition on the responsiveness of perirhinal RS cells, as documented in previous electrophysiological studies (Biella et al. 2001; Martina et al. 2001b). In particular, excitatory connections to PV interneurons and inhibitory connections to RS cells were made with 100 % probability within a radius of 0.75 mm, which ensured that all RS cells were within the inhibitory field of at least one interneuron. SOM cells inhibited all the RS cells within a rostrocaudal distance of 0.75 mm, as well as the PV cells within a rostrocaudal distance of 0.25 mm. SOM cells did not receive inputs from nearby cells, RS or PV. In keeping with prior anatomical and electrophysiological observations, the two types of interneurons targeted different compartments of RS cells (PV, soma; SOM, dendrites; Fino et al. 2013), they formed contrasting connections with each other (SOM cells inhibited PV cells but not the opposite; Pfeffer et al. 2013), and they were differentially innervated by long-range cortical inputs (SOM received such inputs; not PV cells; Adesnik et al. 2012; Zhang et al. 2014).

Synaptic currents, short- and long-term synaptic plasticity

Synaptic currents

As is the case throughout the cerebral cortex, including perirhinal area 36 (Ziakopoulos et al. 2000; Martina et al. 2001a), model inhibitory connections include GABA-A and B receptor-mediated components whereas excitatory synapses are dual glutamatergic AMPA/NMDA synapses. All synapses are assigned maximal and initial conductances (G_{AMPA} , G_{NMDA} , G_{GABA_A} , G_{GABA_B}). These values were equal within each synapse type. AMPA currents were further modified by a plastic weight $W_{i,j}$, as justified below. As is customary in the modeling literature (Dyhrfeld-Johnsen et al. 2007), we compensated for the reduction in network size by increasing synaptic strengths. Conductance values and related details are in sections S.2 and S.3 of suppl. materials.

Short-term synaptic plasticity

Because short-term synaptic depression is ubiquitous between principal cortical neurons, model RS to RS synapses were designed to reproduce this property, based on prior experimental data (Silberberg et al. 2004). We also modeled short-term facilitation at SOM to RS synapses, as seen in the visual cortex (Ma et al. 2012). At facilitating synapses, when two spikes were separated by 10 ms or less, the second EPSP was facilitated. This effect increased progressively as the inter-spike interval decreased, up to a maximal EPSP increase of 20 %, which occurred with inter-spike intervals of 4 ms. For depressing synapses, - when two spikes were separated by 25 ms or less, the second EPSP was depressed. This effect increased progressively as the inter-spike interval decreased, up to a maximal EPSP decrease of 50 %, which occurred with inter-spike intervals of 4 ms. See section S.4 of suppl. materials for how short-term synaptic plasticity was implemented in the model.

Long-term synaptic plasticity

Glutamatergic synapses to principal perirhinal cells can undergo long-term activity-dependent changes in efficacy (McCaffery et al. 1999; Ziakopoulos et al. 1999; Cho et al. 2000, 2001, 2002; Massey et al. 2001, 2004, 2008; Cho and Bashir 2002; Barker et al. 2006a, b; Jo et al. 2008; Bang and Brown 2009). In contrast, to the best of our knowledge, there has been no report of long-term activity-dependent plasticity at connections formed by perirhinal inhibitory neurons. Accordingly, model glutamatergic (but not GABAergic) synapses were endowed with mechanisms allowing long-term activity-dependent plasticity.

It was assumed that activity-dependent changes at inputs to RS cells are expressed postsynaptically, by increases or decreases in AMPA receptor-dependent currents. Based on earlier experimental evidence (Bilkey 1996; Ziakopoulos et al. 1999; Cho et al. 2000, 2001; Jo et al. 2008), these changes in AMPA currents were determined by the competing influence of group I metabotropic glutamate receptors (mGluRs) and NMDA receptors. In particular, activation of group I mGluRs induced long-term depression (LTD) whereas moderate vs strong activation of NMDA receptors induced LTD or long-term potentiation (LTP), respectively. This was implemented as follows. At each excitatory synapse, the AMPA current amplitude was modified by $W_{i,j}$, the plastic weight of the synapse between cell i to cell j . The initial weights of all the synapses are listed in table S.3 of suppl. materials. An increase or decrease in $W_{i,j}$ from the initial value represented potentiation or depression of the synapse. Two Ca^{2+} -dependent mechanisms determined the fate of synaptic weights. Accordingly, two separate Ca^{2+} sources were modeled for each synapse: one pool was supplied by NMDA receptors, and a second by Ca^{2+} release from intracellular stores, under the control of group I mGluRs. Group I mGluRs are known to be located postsynaptically and to have a synaptic (not extra-synaptic) location, as shown in the rat hippocampus with immunocytochemistry (Lujan et al. 1996; Shigemoto et al. 1997). We modeled the impact of mGluR1 activation after experimental studies on the kinetics of these synaptic responses (Marcaggi et al. 2009). Activation of group I mGluRs triggered intracellular release of IP3 via models of binding/unbinding dynamics of synaptic channels reported in the literature with rise and fall times of 100 and 400 ms, respectively. See section S.3 of suppl. materials for details.

Model experiments and statistics

To test the validity of the model, we examined whether it could reproduce the findings of Unal et al. (2012). As in that study, in all model experiments the training protocol consisted of a testing phase “pre-test”, a training phase “training”, and a second testing phase after training “post-test”. During both testing phases, the neocortex was stimulated in the same manner: once at a series of rostro-caudal locations, from 0 to 10 mm, activating 17 neighboring neocortical input neurons at each location (one ‘site’). Three seconds was allowed between the activation of different neocortical sites. To induce activity-dependent plasticity, neocortical inputs from one or more rostrocaudal levels were activated in the following manner: thirty 1-s trains of stimuli (8 Hz), each followed by a 0.5 s stimulus-free period. Below, this stimulation pattern will be termed “theta-frequency stimulation” (TFS). For each modeling

experiment, we ran the model five to ten times from different random seeds and averaged the data. All results are expressed as average \pm SEM. Unless otherwise stated, we used paired *t* tests for statistical comparisons. However, before using this test, we verified that the data to be compared were normally distributed using a Kolmogorov–Smirnov test.

Results

This study investigates the mechanisms of distributed synaptic plasticity underlying associative memory formation in the perirhinal cortex. To this end, guided by previous experimental studies, we developed a model of the perirhinal network that captures salient properties of this cortical region. We first provide a general description of the model's features. Then, to test the model's validity, we examine whether it can reproduce the findings of a prior study on activity-dependent plasticity in the perirhinal cortex (Unal et al. 2012). Finally, we use the model probe mechanisms of associative memory formation in the perirhinal network.

Model overview

The following summarizes the general properties of the model. To minimize computation times while capturing the essence of the perirhinal network (Fig. 1), the number of cells was reduced to 400 principal (glutamatergic, RS) and 120 local-circuit GABAergic neurons (60 PV and 60 SOM) with realistic electroresponsive properties (Fig. 1a1–3). Model PV and SOM cells target different compartments of RS cells (soma and dendrites, respectively), they form contrasting connections with each other (SOM cells inhibit PV cells but not the opposite), and they are differentially innervated by long-range cortical inputs (SOM but not PV cells receive such inputs; Fig. 1b–c). The model features topographically organized glutamatergic inputs from associative temporal cortical areas, modeled with 201 input cells distributed along the rostrocaudal extent of the perirhinal network (Fig. 1b). Note that these “input cells” are in fact just spike trains used for synaptic drive. The model also featured a prominent system of intrinsic longitudinal connections with realistic conduction delays. These long-range connections arise exclusively from principal neurons, they span the entire rostrocaudal extent of the network, and they end on other principal and SOM cells, but not PV neurons. The model also features short-term synaptic dynamics (e.g., synapses between RS cells exhibit short-term depression) and activity-dependent synaptic plasticity (activation of group I mGluRs induces LTD; activation of NMDA receptors induces LTD or LTP

depending on the level of postsynaptic depolarization). Last, LTD and LTP are expressed postsynaptically, by changes in the AMPA conductance of individual synapses.

Response of model neurons to neocortical inputs

Figure 2 shows the response of the model neurons to single neocortical stimuli delivered at the same rostrocaudal level as the recorded cells vs a longitudinally distant site. See suppl. Figure 1 for responses to trains of neocortical stimuli. Responses are shown in two ways: at rest with the full complement of voltage-gated currents (left) or at three

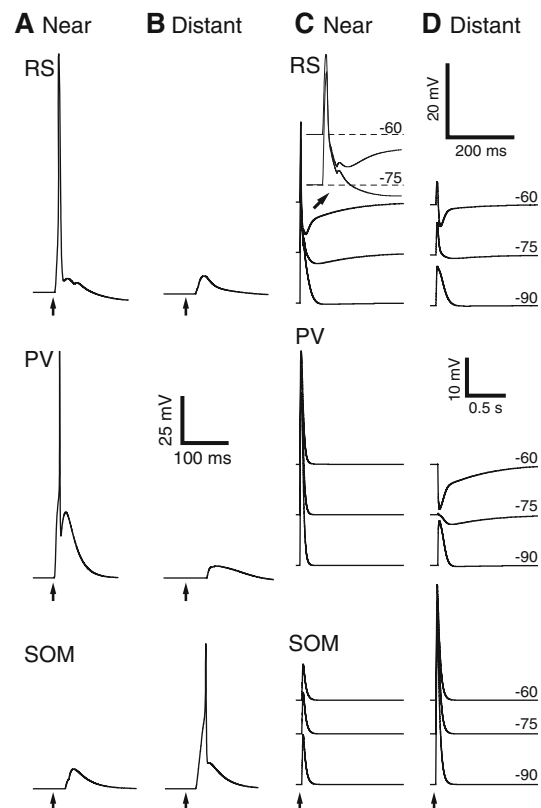


Fig. 2 Response of model neurons to neocortical stimuli applied at nearby and distant neocortical sites. **a, c** Nearby neocortical stimulus. **b, d** Distant neocortical stimulus. *Top to Bottom*: principal regular spiking (RS) neuron, parvalbumin (PV) interneuron, somatostatin (SOM) interneuron. **a, b** Neocortical stimulus applied while neurons were at rest. **c, d** Neocortical stimulus applied while the membrane potential of the cells was set to -60 , -75 , or -90 mV by simulated direct current injection. In **c** and **d**, the voltage-dependent Na^+ conductance was set to *zero* so that synaptic responses could be examined without the contaminating influence of spikes and afterhyperpolarizations. *Inset at top of c*: expanded depiction of RS responses to nearby neocortical stimuli. Note biphasic IPSPs in RS cells with early and late phases mediated by GABA-A and GABA-B receptors, respectively. PV cells fire in response to nearby but not distant neocortical stimuli because they receive short- but not long-range inputs. However, because PV cells receive inhibitory inputs from SOM cells that are excited by distant neocortical stimuli, PV cells exhibit IPSPs in response to distant stimuli

different membrane potentials (right). For the latter, the fast Na^+ conductance of the target cells was set to zero, so the responses could be examined without contamination from spikes and afterhyperpolarizations.

Single stimuli applied at a nearby neocortical site elicited EPSPs that triggered spikes in $45 \pm 8\%$ of RS cells (Fig. 2a, RS). These EPSPs were rapidly curtailed by a biphasic IPSP (Fig. 2c, RS) comprised of an early phase reversing at around -70 mV (GABA-A) and a longer-lasting component with a more negative reversal potential (GABA-B). These IPSPs are due to the supra-threshold activation of many ($50 \pm 14\%$) nearby PV cells (Fig. 2a) by excitatory inputs from RS cells and neocortical input neurons. In contrast, SOM interneurons were never fired by nearby neocortical stimuli (Fig. 2a, SOM). Instead, they exhibited long-latency EPSPs (Fig. 2c, SOM) due to the activation of rostrocaudally distant RS cells that project back to them.

The responses elicited by rostrocaudally distant neocortical stimuli (Fig. 2b) differed drastically from those elicited by nearby stimuli (Fig. 2a). First, RS cells rarely fired in response to distant neocortical stimuli. Second, because the long-range horizontal axons of RS cells do not contact PV neurons, rostrocaudally distant RS cells displayed IPSPs of shorter duration and lower amplitude than seen with nearby neocortical stimuli (Fig. 2b, d, RS). Yet, PV cells displayed long-latency IPSPs due to the activation of SOM cells by longitudinal inputs (Fig. 2b, d, PV). An additional difference between the impacts of nearby vs distant neocortical stimuli resided in the response of SOM cells. Whereas these cells exhibited sub-threshold EPSPs in response to nearby stimuli (Fig. 2a, c, SOM), $47 \pm 17\%$ of them fired in response to distant stimuli (Fig. 2b, d, SOM), due to their innervation by long-range horizontal RS axons.

Dependence of perirhinal plasticity on the spatial distribution of neocortical inputs

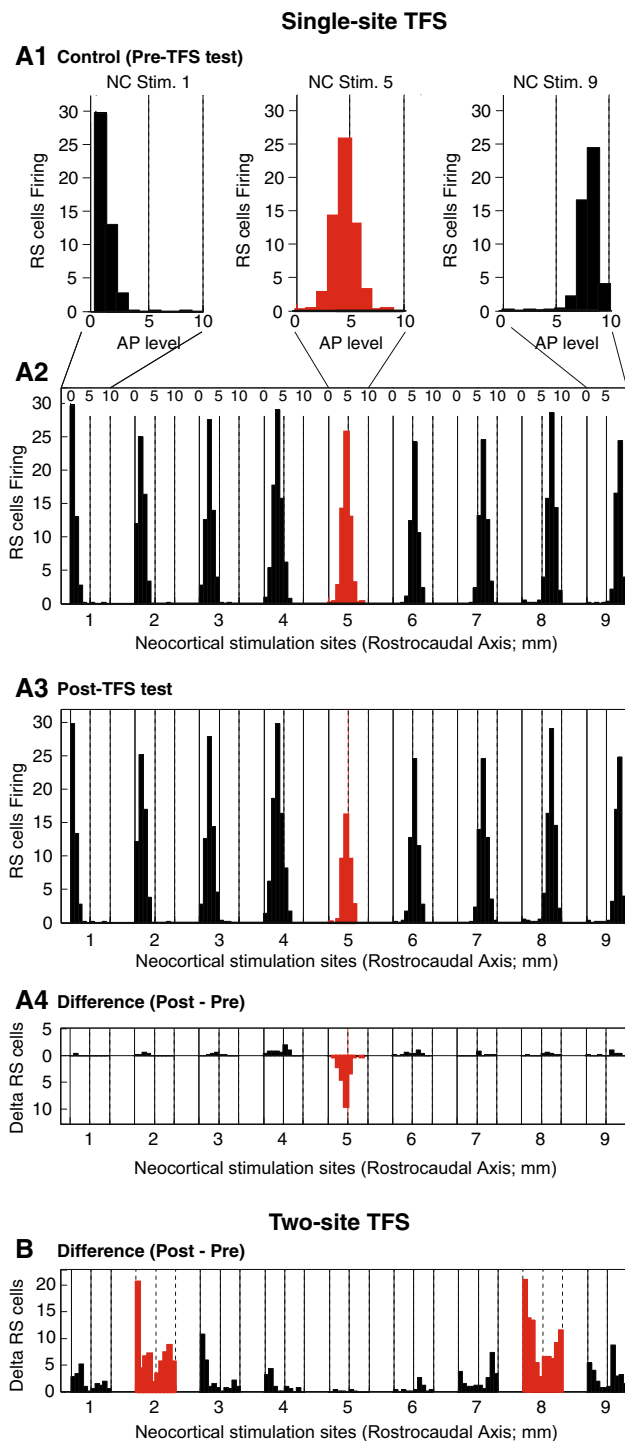
To test the model's validity, we next examined whether it could reproduce the findings of a study on activity-dependent plasticity in perirhinal area 36 of the whole guinea pig brain kept in vitro (Unal et al. 2012). This study examined the activity evoked by temporal neocortical inputs using functional imaging with voltage sensitive dyes and field potential recordings along the rostrocaudal axis of the perirhinal cortex. After obtaining control response amplitudes from each neocortical stimulation site, TFS was applied at one or two distant neocortical sites. Unal et al. (2012) reported that TFS at one neocortical site produced a LTD of evoked responses evoked from the induction site but not from control sites. In contrast, TFS simultaneously applied at two distant neocortical stimulation sites

produced a LTP of perirhinal responses evoked from the induction, but not the control sites. Although the changes in perirhinal responsiveness induced by TFS at one or two neocortical stimulation sites were selective to the induction sites, the changes could be seen throughout the rostrocaudal axis of the perirhinal cortex.

We first simulated TFS application at a single neocortical stimulation site using the perirhinal network model. Such a simulation is shown in Fig. 3a where TFS was applied at neocortical site 5 (red). Before reporting the results of this simulation, we explain the approach used to construct Fig. 3 as the same procedure will be used to illustrate the results of other simulations. The three histograms in Fig. 3a1 plot the number of RS cells firing in response to single neocortical stimuli applied at site 1 (left), site 5 (middle), or site 9 (right). A different color (red) is used for the site 5 histogram because this site will receive TFS in subsequent panels. The *x*-axis of the three histograms shown in Fig. 3a1 corresponds to the rostrocaudal or antero-posterior (AP) axis of the model. By comparing the distribution of activated cells in the three graphs, one can see that the AP level with the most activated cells is always at proximity of the neocortical stimulation site; as the neocortical stimulation site shifts caudally (from the left-most to the right-most histogram), the AP level with the most RS cells firing also shifts caudally. Note that these three histograms actually depict the control responsiveness of the model prior to single-site TFS at site 5. The same three histograms are shown with a compressed *x*-axis below in Fig. 3a2 (oblique lines), along with histograms illustrating the model's responses to other neocortical stimulation sites. Figure 3a2 thus shows the control responsiveness of the model prior to single-site TFS at site 5. Figure 3a3 is organized exactly as Fig. 3a2 but it shows the responsiveness of the model after single-site TFS at site 5. Figure 3a4 simply shows the difference between panels 3a3 and 3a4. Here, negative values mean that fewer RS cells respond after than before single-site TFS at site 5 and thus, that TFS caused a response depression.

As seen experimentally (Unal et al. 2012), we observed that single-site TFS at site 5 caused a marked depression of RS responses evoked from the induction site (Fig. 3a4; $-39 \pm 4\%$ RS cells spiking; paired *t* test, $p < 0.0011$; below, unless otherwise noted, we used paired *t* tests for all statistical comparisons). Further paralleling experimental observations, this depression was restricted to RS cells located at proximity of the stimulation site. Responses to the other stimulation sites remained unchanged ($2 \pm 1\%$; $p = 0.31$).

In contrast with single-site TFS, simultaneous delivery of TFS at two distant neocortical sites (Fig. 3b) produced a potentiation of responses evoked from those sites ($32 \pm 3\%$ RS cells spiking; $p = 0.0002$), as reported in



Unal et al. (2012). Further paralleling experimental findings, the potentiation was seen at all rostrocaudal levels of the model network and was most pronounced for responses elicited from the paired sites; other sites showed only marginal changes ($6 \pm 1\%$; $p = 0.23$). In the Unal et al. (2012) study, it was further observed that delaying the stimulation of one of the two paired sites by half a theta cycle during TFS (or 65 ms) abolished the potentiation of

Fig. 3 Contrasting effects of one- and two-site TFS. **a** One-site TFS. **b** Two-site TFS. **a1** Histograms plotting the number of RS cells firing (y-axis) in response to single neocortical stimuli applied at site 1 (left), site 5 (middle), or site 9 (right). The x-axis of the three histograms corresponds to the rostrocaudal or antero-posterior (AP) axis of the model. In **a2**, the same histograms as in **a1** are shown with a compressed x-axis, along with histograms illustrating the model's responses to other neocortical stimulation sites in control conditions, prior to application of one-site TFS at site 5. The numbers (0, 5, 10) at the top of **a1** refer to these ten target locations and apply to all graphs below. **a3** Same as **a2** but after application of one-site TFS at site 5. **a4** Difference between the histograms shown in **a2** and **a3** (post minus pre TFS). Here, negative values mean that fewer RS cells respond after than before single-site TFS at site 5 and thus, that TFS caused a response depression (**b**) difference between the number of RS cells firing in response to neocortical stimuli before vs after two-site TFS. Red indicates responses elicited by neocortical stimuli where TFS was applied

responses elicited by the paired neocortical inputs. We simulated this experiment and obtained the same result (Suppl. Figure 2).

The Unal et al. (2012) study also reported on the impact of a number of other manipulations such as inactivating long-range connections during two-site TFS as well as the effect of NMDA or group I mGluR antagonists on the activity-dependent plasticity induced by one- or two-site TFS. The model could reproduce the consequences of these various manipulations, as described in Supplementary Fig. 3–4.

Unal et al. (2012) offered the following interpretation for their findings. It is entirely consistent with the phenomena observed in our model. With respect to perirhinal cells in transverse register with the stimulation site, neocortical inputs activate perirhinal PV interneurons, thus limiting the depolarization of principal cells by neocortical afferents. In these conditions, activation of group I mGluRs causes a response depression. In contrast, when these inputs coincide with the activation of a longitudinally distant group of neocortical neurons, responses are shifted toward excitation because long-range longitudinal pathways do not engage PV interneurons. By removing the Mg^{2+} block of NMDA receptors, this stronger depolarization leads to the induction of NMDA-dependent LTP.

Aspects of the model that are critical to reproduce the findings of Unal et al. (2012)

When we developed the current model, we started with single compartment cell models using the Hodgkin-Huxley formulation for currents, and matched their passive properties to prior experimental reports. When using these single compartment cell models in a network, the restriction of locating excitatory and inhibitory inputs on the same compartment turned out to be problematic. When

trying to match the model's behavior to the single- and paired-site TBS cases of Unal et al. (2012) with the same synaptic parameters, network interactions led to runaway excitation. It became apparent that this problem could be alleviated by spatially segregating excitatory and inhibitory inputs, as occurs in the real network. We reasoned that locating inhibitory synapses on somata and excitatory ones on dendrites would result in a relatively more potent inhibition and help control excitation. Implementing these features required the use of multi-compartmental RS cell models. With such multi-compartmental cell models and spatially segregated excitatory and inhibitory synapses, we were able to match the single-site and paired-site results from Unal et al. (2012), but still could not guarantee stability in all cases. Also, reproducing the effects of group I receptor antagonists seen in Unal et al. (2012) remained impossible as it caused runaway excitation. We explored various ways to solve this problem and ultimately found that the most parsimonious approach was to add another type of inhibitory interneuron, this one dendrite-targeting (SOM cells), as present in the real network (see ‘‘methods’’). This solved the problem of runaway excitation and ensured good qualitative, but not quantitative, matches to all the results in Unal et al. (2012). Adding inhibition from SOM to PV cells, as occurs in the real network (Pfeffer et al. 2013), helped overcome this problem, and provided both qualitative and quantitative matches with all the observations in Unal et al. (2012).

Specific perirhinal cells are critical for associative learning: conjunctive cells

Having found that our model could reproduce prior experimental observations, we used it to probe perirhinal mechanisms of associative memory formation. By comparing the responses of RS cells to different neocortical inputs before vs after TFS, we noticed that two-site TFS led to the emergence of RS cells that fired at least one spike in response to independent stimulation of the two paired neocortical inputs. Because no RS cells exhibited this property prior to two-site TFS, we reasoned that these neurons might be more critical than others for the induction and expression of associative plasticity. These cells, hereafter termed conjunctive cells (CCs) were of two types. Roughly half were located at the perirhinal levels adjacent to the paired neocortical stimulation sites (range, 29–44; average, 34.5 ± 2.1 ; $n = 10$; Fig. 4a, red circles) and therefore received direct inputs from one of the two paired sites. The rest (off-site conjunctive cells; range, 27–64, average 42.1 ± 3.6 ; $n = 10$) were not located at perirhinal levels adjacent to the stimulated sites and thus did not receive direct inputs from the paired neocortical sites (Fig. 4a, black circles).

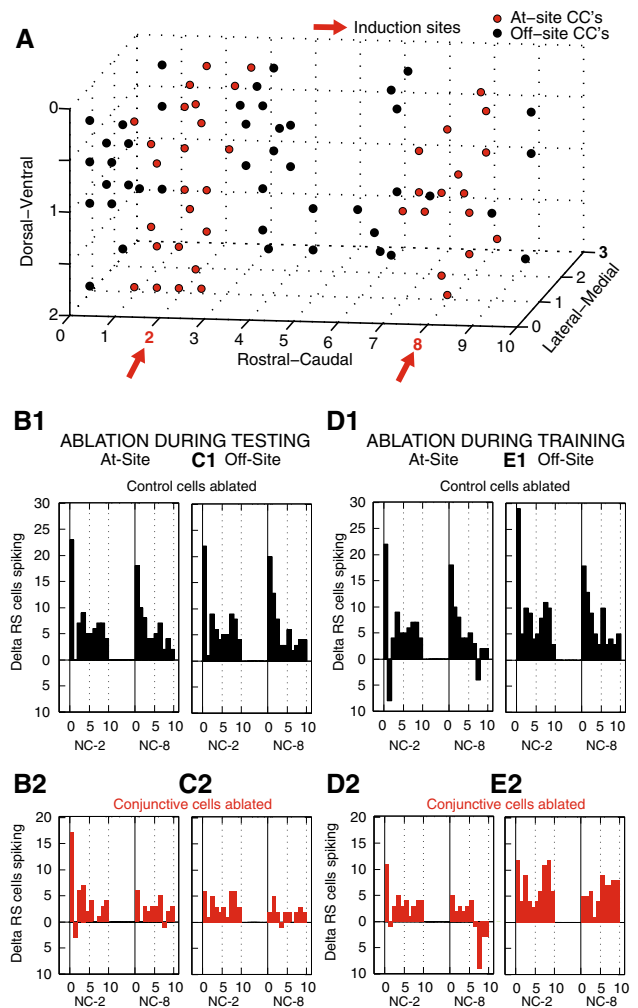


Fig. 4 CCs play a critical role in the induction and expression of plasticity induced by two-site TFS. **a** Location of at-site (red) and off-site (black) CCs. CCs were defined as RS cells that responded to independent stimulation of both paired sites after two-site TFS at sites 2 and 8 (red arrows). **b–e** Histograms showing differences in the number of RS cells spiking (y-axis) after vs before two-site TFS in response to stimulation of site 2 (NC-2) or site 8 (NC-8). The ten target locations in panel b correspond to the ten rostrocaudal positions in panel a. Randomly selected RS cells (panels 1, black) or an equal number of CCs (panels 2, red) were ablated only during testing (**b**, **c**) or training (**d**, **e**). Ablated cells were either located at the same rostrocaudal level as the paired neocortical stimulation sites (**b**, **d**) or not (**c**, **e**). The lateral-medial axis shown in the figure follows the 3D nomenclature of the rodent brain and corresponds to laminar depth, but the curvature has not been shown for convenience

Impact of ablating conjunctive cells

To test whether CCs are more critical than other RS neurons for the associative plasticity induced by two-site TFS, we compared the effect of ablating CCs or an equal number of randomly selected RS cells during two-site TFS only (training phase), or after conditioning (testing phase). These tests were performed separately for at-site vs off-site

Table 3 Intrinsic connectivity (mean \pm SEM) comparison between CCs and control cells with other RS cells that fired during paired TFS

Cell type and total #	# Short-range conn. recd. from spiking RS cells	# Long-range conn. recd. from spiking RS cells	# Short-range conn. made to spiking RS cells	# Long-range conn. made to spiking RS cells
CCs at-site (2 and 8 mm sites), 40	5.65 \pm 0.4	9.95 \pm 0.34	5.4 \pm 0.35	8.2 \pm 0.53
CCs off-site, 44	2.98 \pm 0.3	10.84 \pm 0.42	2.34 \pm 0.3	9.86 \pm 0.53
Control cells at-site (2 and 8 mm sites), 120	3.76 \pm 0.17	5.84 \pm 0.21	4.74 \pm 0.21	6.06 \pm 0.3
Control cells off-site, 196	1.53 \pm 0.11	7.3 \pm 0.21	1.49 \pm 0.1	7.43 \pm 0.27

represents numbers/number

CCs. Note that “ablation” means the cell in question was not allowed to spike and affect other cells by the application of a strong negative current.

Figure 4b–d contrasts the effects of ablating control RS cells (top, black) or CCs (bottom, red) during testing (Fig. 4b, c) or training (Fig. 4d, e) on the number of RS cells firing in response to stimulation of neocortical stimulation sites 2 and 8 after conditioning. Ablation of at-site (Fig. 4b) or off-site (Fig. 4c) CCs during testing produced a significant reduction in the potentiation of responses elicited from the paired sites compared to that seen after removal of control cells at corresponding locations (at-site $p < 0.0001$; off-site, $p = 0.0008$). Similarly, ablating at-site CCs during training (Fig. 4d) produced a significant reduction in the potentiation of responses produced by pairing relative to that seen after removal of at-site control cells (paired t test, $p = 0.0009$). In contrast, ablating off-site CCs during training had little effect (paired t test, $p = 0.17$; Fig. 4d). Further analyzes revealed that this negative finding resulted from the fact that following ablation of off-site CCs, a new set of CCs emerged. For instance, in the particular simulation shown in Fig. 4e2, 33 cells that were not CCs in the control case developed responses to both of the paired sites when training occurred after ablation of the original 40 off-site CCs. This phenomenon suggests that a form of synaptic competition (Kim et al. 2013) takes place between off-site RS cells.

Connectivity of conjunctive cells

To shed light on the properties that determined the emergence of CCs, we compared their inputs and outputs. Overall, relative to other RS cells, there were no significant differences in the number of neocortical inputs they received, in the number of short- or long-range input or output connections they formed with other RS cells or in their connections with PV or SOM interneurons. This was true for both at-site and off-site CCs. When we restricted the comparisons to neocortical inputs recruited by the pairing paradigm, we found that at-site CCs and control RS cells received a similar number of these inputs. Together, these negative findings indicate that there were no a priori

differences in the connectivity of CCs. Rather, these results suggest that CCs emerge out of the specific network interactions that unfold when two groups of neocortical inputs neurons are repeatedly activated during paired-site TFS.

In support of this contention, significant differences in the connectivity of CCs emerged when we examined their intrinsic connections with other RS cells that fired during pairing (Table 3). Indeed, relative to control cells, at-site and off-site CCs received significantly more short- and long-range inputs from RS cells that fired during two-site TFS (for both: $p < 0.0001$; unpaired t tests). Moreover, they contributed significantly more short- and long-range projections to RS cells that fired during two-site TFS (long-range: $p < 0.0001$; short-range: $p = 0.0004$; unpaired t tests).

Reactivation of conjunctive cells

Overall, the above analyzes suggest that CCs play a critical role in the acquisition and expression of associative plasticity. Conceiving this plasticity as a proxy for associative memory, we next asked: are CCs also involved in the recall of associative memories? In the actual network, cells at different rostrocaudal levels of the perirhinal cortex receive different types of sensory information (Room and Groenewegen 1986). Thus, when two sensory inputs are associated in the perirhinal cortex, an optimal storage strategy would be to selectively enhance the responsiveness of RS cells receiving the paired inputs and the connections between them. However, this is not the behavior Unal et al. (2012) observed experimentally or seen in our simulations: the increase in perirhinal responsiveness produced by paired-site TFS is not limited to cells receiving the paired neocortical inputs. It is observed throughout the perirhinal cortex (see Fig. 3b, red).

Thus, when assessing how well (that is, with how much specificity) a “memory” is reactivated, it is important to take into consideration the type of RS cells responding to the reactivating stimulus. Accordingly, below we distinguish between RS cells that acquired new spiking responses to one “plastic cells” or both “conjunctive cells” of the

paired neocortical inputs. Also, we will refer to cells that did not acquire new spiking responses as “non-plastic” cells. Finally, the qualifiers “at-site” or “off-site” will be used for the three terms to indicate whether the cells had access to neocortical inputs from one of the two paired sites during training.

Table 4 lists the relative incidence of at-site and off-site CCs, plastic cells, and non-plastic cells as seen across ten separate runs. Examination of this data reveals that there are nearly as many at-site and off-site cells whose responsiveness to the paired stimuli increases after two-site TFS. On the surface, the diffuse distribution of cells responsive to the paired inputs seems incompatible with selective memory recall: how could an associative memory be retrieved with some measure of selectivity if independent activation of one of the two paired representations recruited so many cells that normally process other inputs. This paradox led us to consider the possibility that at-site or off-site CCs might have unique connections that could promote a more selective reactivation of network, or in other words, that they serve as memory retrieval cells. Here, it should be noted that reactivated at-site plastic cells and CCs, embody the “signal”, and that off-site non-plastic cells, are considered “noise”.

To test this possibility, after two-site TFS, we simultaneously “reactivated” off-site or at site CCs (Fig. 5a1, b1) and compared the impact of these manipulations to that obtained when stimulating an equal number of randomly picked plastic (Fig. 5a2, b2) or non-plastic cells (Fig. 5a3, b3) at the same location. In these simulations ($n = 10$ for each of the 6 cases), random uncorrelated synaptic inputs were injected in all RS cells so that they would fire at an average of ~ 0.6 Hz, as seen in vivo (Collins et al. 1999). On this background, two spikes were elicited in all cells of interest by applying a brief intracellular current pulse (50 ms, 0.18 nA; random onset delay of 1–10 ms; Fig. 5c1) and monitoring the responses elicited in target cells (Fig. 5c2–5). This stimulus can be conceived of as roughly approximating the impact of extrinsic cortical inputs involved in memory retrieval.

Chi square tests revealed a significant dependence in the number of reactivated plastic and CCs at-site and the identity of the stimulated cells (CCs, plastic cells, or control cells) whether the latter were off-site (Fig. 5a; $X^2 = 348.4$, $p < 0.0001$) or at-site (Fig. 5b; $X^2 = 115.8$, $p < 0.0001$). Expectedly, current-evoked firing in non-plastic cells (Fig. 5a3, b3) reactivated very few at-site plastic cells or CCs (≤ 9 % of total) relative to other types of input neurons. Therefore, the following will be restricted

to comparisons between the impact of current-evoked firing in plastic cells vs CCs, off-site or at-site.

To assess which of these two cell classes was most selective in reactivating the associative memory, we compared the incidence of reactivated at-site plastic cells and CCs, embodying the “signal”, and that of off-site non-plastic cells, considered as “noise”, depending on the identity of the input cells. Although other off-site cells could be construed as noise (e.g., off-site plastic cells), we will not consider them below because they served as input cells for some of the stimulation and therefore were not available for recruitment.

We found that whether the input cells were at-site or off-site CCs, they recruited more of the signal cells and less of the off-site non-plastic cells than when the input cells were plastic cells. In particular, when the input cells were off-site (Fig. 5a), current-evoked firing in CCs (Fig. 5a1) recruited 33.4 ± 5.8 % of at-site CCs and 23.1 ± 4.8 % of at-site plastic cells compared to 23.1 ± 6.1 and 14.8 ± 2.9 % of the corresponding cells classes when the input cells were plastic cells (Fig. 5a2). The difference in the combined incidence of at-site plastic cells and CCs as a function of the identity of the input cells was statistically significant ($p = 0.025$). Even though off-site CCs were more effective in recruiting at-site signal cells, they recruited fewer off-site non-plastic cells (13.3 ± 1.6 %) compared to the case when the input cells were off-site plastic cells (21.1 ± 2.3 %; $p = 0.0009$).

Similarly, when the input cells were at-site (site 2 in Fig. 5b), current-evoked firing in CCs (Fig. 5b1) recruited 35.0 ± 6.2 % of at-site CCs and 10.1 ± 1.4 % of at-site plastic cells compared to 15.8 ± 3.7 and 6.1 ± 0.6 % of the corresponding cells classes when the input cells were plastic cells (Fig. 5b2). The difference in the combined incidence of at-site plastic cells and CCs as a function of the identity of the input cells was statistically significant ($p = 0.0013$). As seen when the inputs cells were off-site, even though at-site CCs were more effective in recruiting at-site signal cells, they did not recruit more off-site non-plastic cells (11.3 ± 1.3 %) compared to the case when input cells were at-site plastic cells (12.2 ± 1.6 %; $p = 0.59$). Overall, these results suggest that as a result of paired-site TFS and of the associated activity-dependent plasticity, CCs form a pattern of connections that allows them to preferentially recruit signal cells relative to off-site non-plastic cells. Nevertheless, the pattern of reactivation produced by CCs continued to lack specificity as some of the reactivated cells were not signal neurons.

Table 4 Incidence of CCs, plastic cells, and non-plastic cells with respect to the paired neocortical sites

	CCs	Plastic	Non-plastic	Total
At-site	34.5 ± 2.12	71.6 ± 2.05	53.09 ± 1.66	159.19 ± 5.83
Off-site	42.1 ± 3.6	53.4 ± 3.61	144.5 ± 6.56	240 ± 13.77

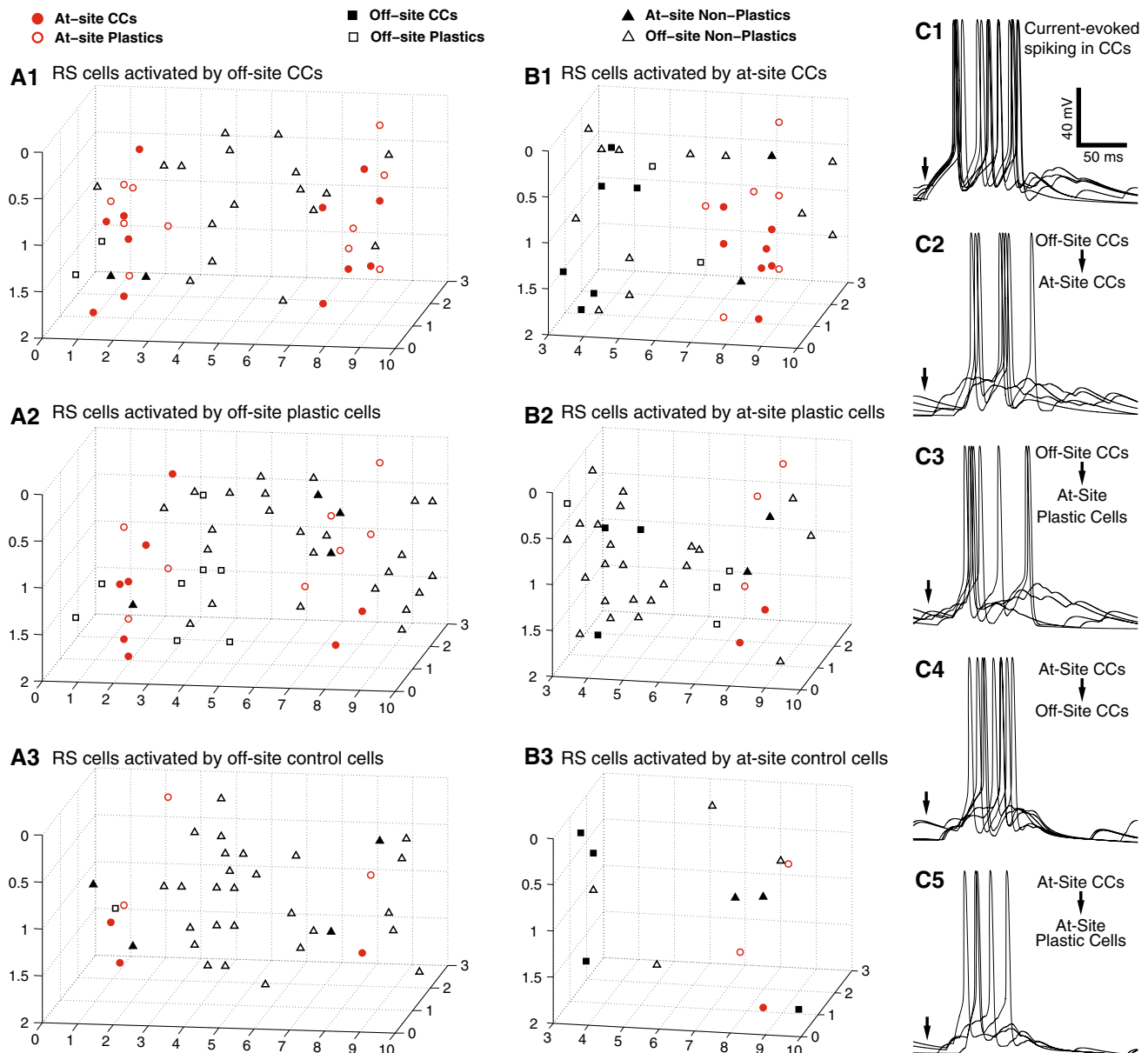


Fig. 5 Firing in CCs after training reactivates plastic neurons. **a** Location of RS cells activated by current-evoked spiking in off-site CCs (**a1**), in an equal number off-site plastic cells (**a2**), or off-site control cells (**a3**). The meaning of the symbols is indicated at the top of the figure. **b** Location of RS cells activated by current-evoked spiking in CCs at-site 2 (**b1**), in an equal number at-site plastic cells (**b2**), or at-site control cells (**b3**). **c** Examples of voltage responses in the various conditions illustrated in a and b. In these simulations,

random uncorrelated synaptic inputs were injected in all cells so that they would fire at an average of ~ 0.6 Hz, as seen in vivo. **c1** Current-evoked spiking in CCs. **c2** Response of at-site CCs to current-evoked spiking in off-site CCs. **c3** Response of at-site plastic (non-conjunctive) cells to current-evoked spiking in off-site CCs. **c4** Response of off-site CCs to current-evoked spiking in at-site CCs. **c5** Response of at-site plastic (non-conjunctive) cells to current-evoked spiking in at-site CCs

Discussion

To shed light on the mechanisms that support associative memory in the perirhinal network, we developed a reduced yet biophysically realistic model of perirhinal area 36. We first assessed the model's validity by testing whether it

could reproduce the findings of a recent study that examined changes in perirhinal responses elicited by activation of neocortical inputs (Unal et al. 2012). The model could reproduce these results. We then used the model to examine the mechanisms that support associative plasticity. Our findings suggest that associative memory formation is

dependent on a specific subset of perirhinal neurons (CCs) that acquire excitatory responses to coincident neocortical inputs and whose reactivation after learning may contribute to memory retrieval.

Relation between activity-dependent plasticity and perirhinal contributions to memory

Depending on stimulation parameters, the perirhinal cortex can exhibit activity-dependent LTP or LTD, as in other cortical regions. For instance, high-frequency (100 Hz) bursts of afferent activity elicit a NMDA-dependent potentiation of perirhinal responses *in vitro* (Bilkey 1996; Ziakopoulos et al. 1999) and *in vivo* (Cousens and Otto 1998). Also, low frequency stimulation produces a Ca^{2+} -dependent LTD or LTP depending on the holding potential during induction (LTD at -70 mV; LTP at -10 mV) (Cho et al. 2001).

The idea emerged that LTD might underlie perirhinal contributions to recognition memory. Indeed, many perirhinal neurons exhibit attenuated responses to previously presented visual stimuli (Brown et al. 1987; Fahy et al. 1993; Li et al. 1993; Miller et al. 1993; Sobotka and Ringo 1993). In contrast, associative memory formation seems to depend on a potentiation of perirhinal responses to paired stimuli (Messinger et al. 2001; Naya et al. 2003). These findings raise the question of how can repeated stimulus presentations lead the same network to express pair coding behavior or familiarity-induced response depression?

It was proposed that the solution resides in the differential relation between neocortical vs perirhinal longitudinal axons with fast-spiking interneurons (Martina et al. 2001b; de Curtis and Pare 2004). Neocortical axons form strong connections with fast-spiking interneurons whereas perirhinal longitudinal axons do not (Martina et al. 2001b; Unal et al. 2013). As a result, repeated activation of neocortical inputs would induce opposite forms of plasticity depending on their spatial distribution. For perirhinal cells in transverse register with the neocortical stimulation site, activation of fast-spiking interneurons limits the depolarization of principal cells by neocortical afferents, favoring LTD. By contrast, when these inputs coincide with the stimulation of rostrocaudally distant neocortical cells, the consequent activation of long-range perirhinal axons shifts the balance toward excitation, promoting the induction of NMDA-dependent LTP. This explanation found support in the findings of Unal et al. (2012) who reported that the polarity and pharmacological dependence of perirhinal plasticity varies depending on the spatial distribution of neocortical inputs. The ability of the current model to reproduce their findings further reinforces this hypothesis.

Synaptic mechanisms of activity-dependent potentiation and depression

The advantage of biophysical models is that they allow manipulations and measurements that would be experimentally impossible or impractical. For example, in the Unal et al. (2012) study, the identity of the synapses supporting the plasticity induced by single- or paired-site TFS remained unclear. In contrast, we could examine the impact of these manipulations on the weight of all model synapses. This analysis revealed that the response depression induced by single-site TFS was mainly due to a decrease in the weight of neocortical inputs to RS cells in transverse register with the neocortical stimulation site. Intrinsic perirhinal connections were barely altered. In contrast, for paired-site TFS, both neocortical and intrinsic glutamatergic synapses supported the response potentiation. Interestingly, there was much heterogeneity in the impact of two-site TFS on the weight of neocortical synapses with roughly equal proportions being potentiated or depressed. This contrasted with the weights of short- and long-range glutamatergic connections, most of which were increased or did not change.

A second example of experimentally impossible manipulation allowed by the model are simulations where one retroactively manipulates the properties of specific cells, in this case CCs. Indeed, we noticed that two-site TFS caused some principal cells (CCs) to acquire suprathreshold responses to independent stimulation of the two paired neocortical inputs. Using the model, we could go back in time to probe the role of these cells by ablating them during training or testing. During testing, ablation of off-site or at-site CCs largely reduced the potentiation of responses elicited from the paired sites relative to that seen after removal of control cells. In contrast, during training, ablation of CCs had little or no effect because a new set of CCs emerged after ablation, suggesting that a form of synaptic competition (Kim et al. 2013) takes place between RS cells.

Significance for memory retrieval

While the perirhinal system of longitudinal connections allows linkage of spatially distributed input patterns, it also poses a challenge for the specificity of stored representations. In the actual network, cells at different rostrocaudal levels of the perirhinal cortex receive different types of sensory information (Room and Groenewegen 1986). However, as seen experimentally (Unal et al. 2012) and in the present simulations, repeated paired activation of distant neocortical inputs not only increased the responsiveness of RS cells receiving the paired inputs but also that of other rostrocaudally distant cells. As a result, subsequent

activation of a potentiated neocortical input not only recruits cells receiving the paired inputs, but also other cells that normally process different types of information.

In an attempt to address this conundrum, we considered the possibility that specific types of principal cells might, as a result of associative plasticity, develop patterns of connections that allow a more selective reactivation of associative memories. To this end, we compared the identity of cells reactivated by current-evoked firing in conjunctive, plastic, and control cells. Relative to other cell types, CCs tended to recruit more of the cells primarily responsible for storing associative memories and less of the ones inadvertently linked to the stored representation. Yet, the reactivation patterns were far from specific.

Together, these observations suggest that the perirhinal network is dependent on its targets to increase the specificity of stored representations. A prime candidate for this function is the entorhinal cortex, a major recipient of perirhinal axons (Witter et al. 1986; Insausti et al. 1987; Suzuki and Amaral 1994; Burwell and Amaral 1998a, b). Indeed, considerable experimental and computational evidence supports the notion that increases in the specificity of stored representations could be produced by attractor states within populations of entorhinal neurons for instance (see Akrami et al. 2009). Clues as to how entorhinal neurons might fulfill this role come from the dependence of TBS-induced changes in perirhinal responsiveness on rostro-caudal distance from the paired neocortical sites: the increase in responsiveness was more pronounced at perirhinal sites receiving the paired inputs and at immediately adjacent rostrocaudal levels than at more distant sites. Thus, it is possible that the entorhinal network enhances the rostrocaudal differentiation in perirhinal activation patterns. Consistent with this suggestion, prior physiological studies have emphasized that perirhinal-entorhinal interactions are regulated by a powerful inhibitory system, allowing for a selection of relevant inputs (de Curtis and Pare 2004). Thus, an important question for future investigations will be to analyze how interactions among the rhinal cortices participate in the formation and recall of associative memories.

Conclusions

Our modeling experiments predict that the formation and reactivation of associative memories in the perirhinal cortex are critically dependent on a subset of principal neurons, termed CCs. When associative plasticity is induced, these cells acquire supra-threshold response to independent stimulation of the paired inputs. Although CCs are required for the post-learning reactivation of the activity patterns that subtend associative memories, this

property is not due to a priori differences in their connectivity. Rather, our results suggest that CCs emerge from competitive synaptic interactions that unfold during the induction protocol. In keeping with this, pre-learning ablation of CCs do not prevent associative plasticity as the original CCs are replaced by new ones. While the retroactive manipulations we used to demonstrate this will never be possible experimentally, post-learning treatments aiming at selectively reducing or enhancing the activity of CCs are theoretically possible. Such manipulations should respectively interfere with vs enhance associative memory recall. Given recent progress in genetic engineering methods for selectively manipulating specific subtypes of neurons, we are confident that our predictions will soon be tested.

Acknowledgments This research was supported in part by Grants from the National Institute of Mental Health (MH073610 and MH-098738 to DP and MH087755 to SSN).

Compliance with ethical standards

Conflict of interest The authors declare no competing financial interests.

References

- Adesnik H, Bruns W, Taniguchi H, Huang ZJ, Scanziani M (2012) A neural circuit for spatial summation in visual cortex. *Nature* 490:226–231
- Aggleton JP, Hunt PR, Rawlins JN (1986) The effects of hippocampal lesions upon spatial and non-spatial tests of working memory. *Behav Brain Res* 19:133–146
- Akrami A, Liu Y, Treves A, Jagadeesh B (2009) Converging neuronal activity in inferior temporal cortex during the classification of morphed stimuli. *Cereb Cortex* 19:760–776
- Ball JM, Hummos A, Nair SS (2012) Role of sensory input distribution and intrinsic connectivity in lateral amygdala during auditory fear conditioning. *Neuroscience* 224:249–267
- Bang SJ, Brown TH (2009) Muscarinic receptors in perirhinal cortex control trace conditioning. *J Neurosci* 29:4346–4350
- Barker GRI, Bashir ZI, Brown MW, Warburton EC (2006a) A temporally distinct role for group I and group II metabotropic glutamate receptors in object recognition memory. *Learn Mem* 13:178–186
- Barker GRI, Warburton EC, Koder T, Dolman NP, More JCA, Aggleton JP, Bashir ZI, Auberson YP, Jane DE, Brown MW (2006b) The different effects on recognition memory of perirhinal kainate and NMDA glutamate receptor antagonism: implications for underlying plasticity mechanisms. *J Neurosci* 26:3561–3566
- Beggs JM, Kairiss EW (1994) Electrophysiology and morphology of neurons in rat perirhinal cortex. *Brain Res* 665:18–32
- Biella G, Uva L, de Curtis M (2001) Network activity evoked by neocortical stimulation in area 36 of the guinea pig perirhinal cortex. *J Neurophysiol* 86:164–172
- Biella G, Uva L, de Curtis M (2002) Propagation of neuronal activity along the neocortical-perirhinal-entorhinal pathway in the guinea pig. *J Neurosci* 22:9972–9979

- Bilkey DK (1996) Long-term potentiation in the in vitro perirhinal cortex displays associative properties. *Brain Res* 733:297–300
- Bogacz R, Brown MW (2003) An anti-Hebbian model of familiarity discrimination in the perirhinal cortex. *Neurocomputing* 52:1–6
- Brown MW, Wilson FAW, Riches IP (1987) Neuronal evidence that inferomedial temporal cortex is more important than hippocampus in certain processes underlying recognition memory. *Brain Res* 409:158–167
- Buckley MJ, Gaffan D (1998) Learning and transfer of object-reward associations and the role of the perirhinal cortex. *Behav Neurosci* 112:15–23
- Burwell RD (2000) The parahippocampal region: corticocortical connectivity. *Ann N Y Acad Sci* 911:25–42
- Burwell RD, Amaral DG (1998a) Cortical afferents of the perirhinal, postrhinal, and entorhinal cortices of the rat. *J Comp Neurol* 398:179–205
- Burwell RD, Amaral DG (1998b) Perirhinal and postrhinal cortices of the rat: interconnectivity and connections with the entorhinal cortex. *J Comp Neurol* 391:293–321
- Burwell RD, Witter MP, Amaral DG (1995) Perirhinal and postrhinal cortices of the rat: a review of the neuroanatomical literature and comparison with findings from the monkey brain. *Hippocampus* 5:390–408
- Bush PC, Sejnowski TJ (1993) Reduced compartmental models of neocortical pyramidal cells. *J Neurosci Methods* 46:159–166
- Cho K, Bashir ZI (2002) Cooperation between mglu receptors: a depressing mechanism? *Trends Neurosci* 25:405–411
- Cho K, Kemp N, Noel J, Aggleton JP, Brown MW, Bashir ZI (2000) A new form of long-term depression in the perirhinal cortex. *Nat Neurosci* 3:150–156
- Cho K, Aggleton JP, Brown MW, Bashir ZI (2001) An experimental test of the role of postsynaptic calcium levels in determining synaptic strength using perirhinal cortex of rat. *J Physiol* 532:459–466
- Cho K, Brown MW, Bashir ZI (2002) Mechanisms and physiological role of enhancement of mGlu5 receptor function by group II mGlu receptor activation in rat perirhinal cortex. *J Physiol* 540:895–906
- Collins DR, Lang EJ, Paré D (1999) Spontaneous activity of the perirhinal cortex in behaving cats. *Neuroscience* 89:1025–1039
- Cousens G, Otto TA (1998) Induction and transient suppression of longterm potentiation in the peri- and postrhinal cortices following theta-related stimulation of hippocampal field CA1. *Brain Res* 780:95–101
- Cowell RA (2012) Computational models of perirhinal cortex function. *Hippocampus* 22:1952–1964
- Cowell RA, Bussey TJ, Saksida LM (2006) Why does brain damage impair memory? A connectionist model of object recognition memory in perirhinal cortex. *J Neurosci* 26:12186–12197
- Cowell RA, Bussey TJ, Saksida LM (2010) Functional dissociations within the ventral object processing pathway: cognitive modules or a hierarchical continuum? *J Cogn Neurosci* 22:2460–2479
- D'Antuono M, Biagini G, Tancredi V, Avoli M (2001) Electrophysiology of regular firing cells in the rat perirhinal cortex. *Hippocampus* 11:662–672
- De Curtis M, Pare D (2004) The rhinal cortices: a wall of inhibition between the neocortex and hippocampus. *Prog Neurobiol* 74:101–110
- Deacon TW, Eichenbaum H, Rosenberg P, Eckmann KW (1983) Afferent connections of the perirhinal cortex in the rat. *J Comp Neurol* 220:168–190
- Dickson CT, Magistretti J, Shalinsky MH, Fransén E, Hasselmo ME, Alonso A (2000) Properties and role of ih in the pacing of subthreshold oscillations in entorhinal cortex layer II neurons. *J Neurophysiol* 83:2562–2579
- Dyhrfeld-Johnsen J, Santhakumar V, Morgan RJ, Huerta R, Tsimring L, Soltesz I (2007) Topological determinants of epileptogenesis in large-scale structural and functional models of the dentate gyrus derived from experimental data. *J Neurophysiol* 97:1566–1587
- Eichenbaum H, Schoenbaum G, Young B, Bunsey M (1996) Functional organization of the hippocampal memory system. *Proc Natl Acad Sci USA* 93:13500–13507
- Fahy FL, Riches IP, Brown MW (1993) Neuronal activity related to visual recognition memory: long-term memory and the encoding of recency and familiarity information in the primate anterior and medial inferior temporal cortex and rhinal cortex. *Exp Brain Res* 96:457–472
- Faulkner B, Brown TH (1999) Morphology and physiology of neurons in the rat perirhinal-lateral amygdala area. *J Comp Neurol* 411:613–642
- Fino E, Packer AM, Yuste R (2013) The logic of inhibitory connectivity in the neocortex. *Neuroscientist* 19:228–237
- Fransen E, Alonso AA, Hasselmo ME (2002) Simulations of the role of the muscarinic-activated calcium-sensitive nonspecific cation current INCM in entorhinal neuronal activity during delayed matching tasks. *J Neurosci* 22:1081–1097
- Fransén E, Alonso AA, Dickson CT, Magistretti J, Hasselmo ME (2004) Ionic mechanisms in the generation of subthreshold oscillations and action potential clustering in entorhinal layer II stellate neurons. *Hippocampus* 14:368–384
- Fransén E, Tahvildari B, Egorov AV, Hasselmo ME, Alonso AA (2006) Mechanism of graded persistent cellular activity of entorhinal cortex layer V neurons. *Neuron* 49:735–746
- Furtak SC, Wei S-M, Agster KL, Burwell RD (2007) Functional neuroanatomy of the parahippocampal region in the rat: the perirhinal and postrhinal cortices. *Hippocampus* 17:709–722
- Gaffan D, Murray EA (1992) Monkeys (*Macaca fascicularis*) with rhinal cortex ablations succeed in object discrimination learning despite 24-h intertrial intervals and fail at matching to sample despite double sample presentations. *Behav Neurosci* 106:30–38
- Goulet S, Murray EA (2001) Neural substrates of crossmodal association memory in monkeys: the amygdala versus the anterior rhinal cortex. *Behav Neurosci* 115:271–284
- Gupta A, Wang Y, Markram H (2000) Organizing principles for a diversity of GABAergic interneurons and synapses in the neocortex. *Science* 287:273–278
- Hemond P, Epstein D, Boley A, Migliore M, Ascoli GA, Jaffe DB (2008) Distinct classes of pyramidal cells exhibit mutually exclusive firing patterns in hippocampal area CA3b. *Hippocampus* 18:411–424
- Higuchi S, Miyashita Y (1996) Formation of mnemonic neuronal responses to visual paired associates in inferotemporal cortex is impaired by perirhinal and entorhinal lesions. *Proc Natl Acad Sci USA* 93:739–743
- Hummos A, Franklin CC, Nair SS (2014) Intrinsic mechanisms stabilize encoding and retrieval circuits differentially in a hippocampal network model. *Hippocampus* 24:1430–1448
- Insausti R, Amaral DG, Cowan WM (1987) The entorhinal cortex of the monkey: II Cortical afferents. *J Comp Neurol* 264:356–395
- Jo J, Heon S, Kim MJ, Son GH, Park Y, Henley JM, Weiss JL, Sheng M, Collingridge GL, Cho K (2008) Metabotropic glutamate receptor-mediated ltd involves two interacting Ca²⁺ sensors, NCS-1 and PICK1. *Neuron* 60:1095–1111
- Kawaguchi Y, Kondo S (2002) Parvalbumin, somatostatin and cholecystokinin as chemical markers for specific GABAergic interneuron types in the rat frontal cortex. *J Neurocytol* 31:277–287
- Kim D, Pare D, Nair SS (2013) Assignment of model amygdala neurons to the fear memory trace depends on competitive synaptic interactions. *J Neurosci* 33:14354–14358

- Kim D, Samarth P, Feng F, Pare D, Nair S (2015) Synaptic competition in the lateral amygdala and the stimulus specificity of conditioned fear: a biophysical modeling study. *Brain Struct Funct* 1–20
- Klausberger T, Somogyi P (2008) Neuronal diversity and temporal dynamics: the unity of hippocampal circuit operations. *Science* 321:53–57
- Leonard BW, Amaral DG, Squire LR, Zola-Morgan S (1995) Transient memory impairment in monkeys with bilateral lesions of the entorhinal cortex. *J Neurosci* 15:5367–5659
- Li L, Miller EK, Desimone R (1993) The representation of stimulus familiarity in anterior inferior temporal cortex. *J Neurophysiol* 69:1918–1929
- Lujan R, Nusser Z, Roberts JDB, Shigemoto R, Somogyi P (1996) Perisynaptic location of metabotropic glutamate receptors mGluR1 and mGluR5 on dendrites and dendritic spines in the rat hippocampus. *Eur J Neurosci* 8:1488–1500
- Ma Y, Hu H, Berrebi AS, Mathers PH, Agmon A (2006) Distinct subtypes of somatostatin-containing neocortical interneurons revealed in transgenic mice. *J Neurosci* 26(19):5069–5082
- Ma Y, Hu H, Agmon A (2012) Short-term plasticity of unitary inhibitory-to-inhibitory synapses depends on the presynaptic interneuron subtype. *J Neurosci* 32:983–988
- Marcaggi P, Mutoh H, Dimitrov D, Beato M, Knöpfel T (2009) Optical measurement of mGluR1 conformational changes reveals fast activation, slow deactivation, and sensitization. *Proc Natl Acad Sci USA* 106(27):11388–11393
- Markram H, Lübke J, Frotscher M, Sakmann B (1997) Regulation of synaptic efficacy by coincidence of postsynaptic APs and EPSPs. *Science* 275(5297):213–215
- Martina M, Royer S, Pare D (2001a) Cell-type-specific GABA responses and chloride homeostasis in the cortex and amygdala. *J Neurophysiol* 86:2887–2895
- Martina M, Royer S, Pare D (2001b) Propagation of neocortical inputs in the perirhinal cortex. *J Neurosci* 21:2878–2888
- Massey PV, Bhabra G, Cho K, Brown MW, Bashir ZI (2001) Activation of muscarinic receptors induces protein synthesis-dependent long-lasting depression in the perirhinal cortex. *Eur J Neurosci* 14:145–152
- Massey PV, Johnson BE, Moulton PR, Auberson YP, Brown MW, Molnar E, Collingridge GL, Bashir ZI (2004) Differential roles of NR2A and NR2B-containing NMDA receptors in cortical long-term potentiation and long-term depression. *J Neurosci* 24:7821–7828
- Massey PV, Phythian D, Narduzzo K, Warburton EC, Brown MW, Bashir ZI (2008) Learning-specific changes in long-term depression in adult perirhinal cortex. *J Neurosci* 28:7548–7554
- McCaffery B, Cho K, Bortolotto ZA, Aggleton JP, Brown MW, Conquet F, Collingridge GL, Bashir ZI (1999) Synaptic depression induced by pharmacological activation of metabotropic glutamate receptors in the perirhinal cortex in vitro. *Neuroscience* 93:977–984
- McGann JP, Moyer JR Jr, Brown TH (2001) Predominance of late-spiking neurons in layer VI of rat perirhinal cortex. *J Neurosci* 21:4969–4976
- Messinger A, Squire LR, Zola SM, Albright TD (2001) Neuronal representations of stimulus associations develop in the temporal lobe during learning. *Proc Natl Acad Sci USA* 98:12239–12244
- Meunier M, Bachevalier J, Mishkin M, Murray EA (1993) Effects on visual recognition of combined and separate ablations of the entorhinal and perirhinal cortex in rhesus monkeys. *J Neurosci* 13:5418–5432
- Meunier M, Hadfield W, Bachevalier J, Murray EA (1996) Effects of rhinal cortex lesions combined with hippocampectomy on visual recognition memory in rhesus monkeys. *J Neurophysiol* 75:1190–1205
- Migliore M (2003) On the integration of subthreshold inputs from perforant path and schaffer collaterals in hippocampal CA1 pyramidal neurons. *J Comput Neurosci* 14:185–192
- Migliore M, Cook EP, Jaffe DB, Turner DA, Johnston D (1995) Computer simulations of morphologically reconstructed CA3 hippocampal neurons. *J Neurophysiol* 73:1157–1168
- Migliore M, Hoffman DA, Magee JC, Johnston D (1999) Role of an a-type K⁺ conductance in the back-propagation of action potentials in the dendrites of hippocampal pyramidal neurons. *J Comput Neurosci* 7:5–15
- Miller EK, Li L, Desimone R (1993) Activity of neurons in anterior inferior temporal cortex during a short-term memory task. *J Neurosci* 13:1460–1478
- Moyer JR, McNay EC, Brown TH (2002) Three classes of pyramidal neurons in layer V of rat perirhinal cortex. *Hippocampus* 12:218–234
- Murray EA, Mishkin M (1986) Visual recognition in monkeys following rhinal cortical ablations combined with either amygdectomy or hippocampectomy. *J Neurosci* 6:1991–2003
- Murray EA, Gaffan EA, Mishkin M (1993) Neural substrate of visual stimulus-stimulus association in rhesus monkey. *J Neurosci* 13:4549–4561
- Murray EA, Graham KS, Gaffan D (2005) Perirhinal cortex and its neighbours in the medial temporal lobe: contributions to memory and perception. *Q J Exp Psychol B* 58:378–396
- Naya Y, Yoshida M, Miyashita Y (2003) Forward processing of long-term associative memory in monkey. *J Neurosci* 23:2861–2871
- Parker A, Gaffan D (1998) Lesions of the primate rhinal cortex cause deficits in flavour-visual associative memory. *Behav Brain Res* 93:99–105
- Pelletier JG, Pare D (2002) Uniform range of conduction times from the lateral amygdala to distributed perirhinal sites. *J Neurophysiol* 87:1213–1221
- Pfeffer CK, Xue M, He M, Huang ZJ, Scanziani M (2013) Inhibition of inhibition in visual cortex: the logic of connections between molecularly distinct interneurons. *Nat Neurosci* 16:1068–1076
- Riches IP, Wilson FA, Brown MW (1991) The effects of visual stimulation and memory on neurons of the hippocampal formation and the neighboring parahippocampal gyrus and inferior temporal cortex of the primate. *J Neurosci* 11:1763–1779
- Rolls ET, Cahusac P, Feigenbaum JD, Miyashita Y (1993) Responses of single neurons in the hippocampus of the macaque related to recognition memory. *Exp Brain Res* 93:299–306
- Room P, Groenewegen HJ (1986) Connections of the parahippocampal cortex. I. Cortical afferents. *J Comp Neurol* 251:415–450
- Rudy B, Fishell G, Lee S, Hjerling-Leffler J (2011) Three groups of interneurons account for nearly 100 % of neocortical GABAergic neurons. *Dev Neurobiol* 71:45–61
- Seoane A, Massey PV, Keen H, Bashir ZI, Brown MW (2009) L-type voltage-dependent calcium channel antagonists impair perirhinal long-term recognition memory and plasticity processes. *J Neurosci* 29:9534–9544
- Shigemoto R, Kinoshita A, Wada E, Nomura S, Ohishi H, Takada M, Flor PJ, Neki A, Abe T, Nakanishi S, Mizuno N (1997) Differential presynaptic localization of metabotropic glutamate receptor subtypes in the rat hippocampus. *J Neurosci* 17:7503–7522
- Shouval HZ, Bear MF, Cooper LN (2002) A unified model of NMDA receptor-dependent bidirectional synaptic plasticity. *Proc Natl Acad Sci USA* 99:10831–10836
- Silberberg G, Wu C, Markram H (2004) Synaptic dynamics control the timing of neuronal excitation in the activated neocortical microcircuit. *J Physiol* 556:19–27
- Sobotka S, Ringo JL (1993) Investigation of long-term recognition and association memory in unit responses from inferotemporal cortex. *Exp Brain Res* 96:28–38

- Sohal V, Hasselmo ME (2000) A model for experience-dependent changes in the responses of inferotemporal neurons. *Network Comp Neural Syst* 11:169–190
- Storm JF (1988) Temporal integration by a slowly inactivating K^+ current in hippocampal neurons. *Nature* 336:379–381
- Suzuki WA, Amaral DG (1994) Perirhinal and parahippocampal cortices of the macaque monkey: cortical afferents. *J Comp Neurol* 350:497–533
- Suzuki WA, Zola-Morgan S, Squire LR, Amaral DG (1993) Lesions of the perirhinal and parahippocampal cortices in the monkey produce long-lasting memory impairment in the visual and tactual modalities. *J Neurosci* 13:2430–2451
- Unal G, Apergis-Schoute J, Pare D (2012) Associative properties of the perirhinal network. *Cereb Cortex* 22:1318–1332
- Unal G, Pare JF, Smith Y, Pare D (2013) Differential connectivity of short- vs long-range extrinsic and intrinsic cortical inputs to perirhinal neurons. *J Comp Neurol* 521:2538–2550
- Uva L, Gruschke S, Biella G, Curtis Md, Witter MP (2004) Cytoarchitectonic characterization of the parahippocampal region of the guinea pig. *J Comp Neurol* 474:289–303
- Wan H, Warburton EC, Zhu XO, Koder TJ, Park Y, Aggleton JP, Cho K, Bashir ZI, Brown MW (2004) Benzodiazepine impairment of perirhinal cortical plasticity and recognition memory. *Eur J Neurosci* 20:2214–2224
- Warburton EC, Koder T, Cho K, Massey PV, Duguid G, Barker GRI, Aggleton JP, Bashir ZI, Brown MW (2003) Cholinergic neurotransmission is essential for perirhinal cortical plasticity and recognition memory. *Neuron* 38:987–996
- Witter MP, Room P, Groenewegen HJ, Lohman AHM (1986) Connections of the parahippocampal cortex in the cat. V. Intrinsic connections; comments on input/output connections with the hippocampus. *J Comp Neurol* 252:78–94
- Witter MP, Wouterlood FG, Naber PA, Van Haeften T (2000) Anatomical organization of the parahippocampal-hippocampal network. *Ann Ny Acad Sci* 911:1–24
- Xiang JZ, Brown MW (1998) Differential neuronal encoding of novelty, familiarity and recency in regions of the anterior temporal lobe. *Neuropharmacology* 37:657–676
- Zhang S, Xu M, Kamigaki T, Hoang Do JP, Chang WC, Jenvay S, Miyamichi K, Luo L, Dan Y (2014) Selective attention. Long-range and local circuits for top-down modulation of visual cortex processing. *Science* 345:660–665
- Ziakopoulos Z, Tillett CW, Brown MW, Bashir ZI (1999) Input- and layer-dependent synaptic plasticity in the rat perirhinal cortex in vitro. *Neuroscience* 92:459–472
- Ziakopoulos Z, Brown MW, Bashir ZI (2000) GABAB receptors mediate frequency-dependent depression of excitatory potentials in rat perirhinal cortex in vitro. *Eur J Neurosci* 12:803–809
- Zola-Morgan S, Squire LR, Amaral DG, Suzuki WA (1989) Lesions of perirhinal and parahippocampal cortex that spare the amygdala and hippocampal formation produce severe memory impairment. *J Neurosci* 9:4355–4370